Mon. Not. R. Astron. Soc. **387,** 1489–1498 (2008) doi:10.1111/j.1365-2966.2008.13358.x

A systematic look at the very high and low/hard state of GX 339−4: constraining the black hole spin with a new reflection model

R. C. Reis,[1⋆] A. C. Fabian,[1] R. R. Ross,[2] G. Miniutti,[1,5] J. M. Miller[3] and C. Reynolds[4]

[1]*Institute of Astronomy, Madingley Road, Cambridge CB3 0HA*
[2]*Physics Department, College of the Holy Cross, Worcester, MA 01610, USA*
[3]*Department of Astronomy, University of Michigan, 500 Church Street, Ann Arbor, MI 48109, USA*
[4]*Department of Astronomy, The University of Maryland, College Park, MD 20742, USA*
[5]*Laboratoire Astroparticule et Cosmologie (APC), UMR 7164, 10 Rue A. Domon et L. Duquet, 75205 Paris, France*

Accepted 2008 April 17. Received 2008 April 17; in original form 2008 March 7

ABSTRACT

We present a systematic study of GX 339−4 in both its very high and low hard states from simultaneous observations made with *XMM–Newton* and *RXTE* in 2002 and 2004. The X-ray spectra of both these extreme states exhibit strong reflection signatures, with a broad, skewed Fe Kα line clearly visible above the continuum. Using a newly developed, self-consistent reflection model which implicitly includes the blackbody radiation of the disc as well as the effect of Comptonization, blurred with a relativistic line function, we were able to infer the spin parameter of GX 339−4 to be 0.935 ± 0.01 (statistical) ± 0.01 (systematic) at 90 per cent confidence. We find that both states are consistent with an ionized thin accretion disc extending to the innermost stable circular orbit around the rapidly spinning black hole.

Key words: accretion, accretion disc – black hole physics – X-rays: individual: GX 339−4.

1 INTRODUCTION

X-ray spectra of Galactic black hole candidates (GBHCs) are an important tool in the studies of the inner regions of accretion flow around black holes (BHs), providing information on both the geometry of the accretion disc and on intrinsic physical parameters such as BH mass and spin.

The spectrum can be explained by the combination of a quasi-thermal blackbody component[1] caused by radiatively efficient accretion through a disc (Shimura & Takahara 1995; Merloni, Fabian & Ross 2000), a power-law component due to inverse Compton scattering of the soft thermal disc photons in a cloud of hot electrons or 'corona' (Zdziarski & Gierlinski 2004), and a reflection component (Ross & Fabian 1993). The latter arises as hard emission from the corona irradiates the cooler disc below and results in 'reflection signatures' consisting of fluorescent and recombination emission lines as well as absorption features. The most prominent of these 'signatures' is the broad, skewed Fe Kα line observed in a number of GBHCs and active galactic nuclei (AGN, see Miller 2007 for a recent review) indicative of reflection from the innermost regions of an accretion disc.

In the inner regions of an accretion disc the iron Kα line shape is distorted by various relativistic effects such as gravitational redshift, light-bending, frame-dragging and Doppler shifts, with the effects becoming more prominent the closer the line is emitted to the event horizon (Fabian et al. 1989; Laor 1991; Fabian et al. 2000). In the case of an accretion disc around a non-spinning Schwarzchild BH, stable circular orbits can only extend down to the radius of marginal stability, $r_{\rm ms} = 6.0 r_{\rm g}$ where $r_{\rm g} = GM/c^2$. This radius depends on the spin parameter a/M, and decreases to $\approx 1.24 r_{\rm g}$ for a maximally rotating ($a/M \approx 0.998$) Kerr BH (Thorne 1974). By making the standard assumption that the emission region extends down to the radius of marginal stability (i.e. $r_{\rm in} = r_{\rm ms}$) one can obtain an estimate on the dimensionless spin parameter (Bardeen, Press & Teukolsky 1972; Reynolds & Fabian 2008).

GX 339−4 is a dynamically constrained ($M_{\rm BH} \geqslant 6.0\,{\rm M}_{\odot}$; Hynes et al. 2003; Munoz-Darias, Casares & Martinez-Pais 2008) recurrent black hole binary (BHB). Its distance has been estimated at 8 kpc (Zdziarski et al. 2004). Observations have been made on multiple occasions in various spectral states from the 'low/hard' to the 'very high state' (VHS; for a recent review on the different spectral states see e.g. McClintock & Remillard 2006). In both the VHS and the low/hard state (LHS) GX 339−4 shows a power-law spectra, with photon index $\Gamma \sim 2.5$–2.7 and 1.4–1.5, respectively (Miller et al. 2004, 2006, hereafter M1 and M2; for a recent analysis of *Suzaku* observation in the 'intermediate' state see Miller et al. 2008), as well as the presence of a quasi-thermal disc component, usually described by a multicolour disc blackbody model (MCD; Mitsuda et al. 1984). In both cases, the fluorescent Fe Kα features have been modelled by the addition of a LAOR relativistic line (Laor 1991) plus an ionized disc reflection component (PEXRIV, Magdziarz

⋆E-mail: rcr36@ast.cam.ac.uk

[1] The term quasi-thermal blackbody applies here to the local emission at the surface of the accretion disc. Due to opacity effects it is broader than a true blackbody spectrum.

& Zdziarski 1995). In this manner, Miller et al. (2004, 2006) measured $r_{\rm in} \sim 2.0$–$3.0\,r_{\rm g}$ and $r_{\rm in} \sim 3.0$–$5.0 r_{\rm g}$, for the VHS and LHS, respectively.

It has long been known that the reflection in a BHB system cannot be mimicked simply by adding a blackbody component to the reflection spectrum from an otherwise cool disc. Compton broadening of the iron Kα line is of greater importance in warm accretion discs and should thus modify the spectral behaviour of BHB compared to that of AGN. In this paper we undertake a systematic reanalysis of the VHS and LHS of GX 339−4, as reported by Miller et al. (2004, 2006). We employ the self-consistent reflection model developed by Ross & Fabian (2007), where blackbody radiation entering the accretion disc surface layers from below, as well as the effect of Comptonization, is implicitly included in the model.

Our method of measuring the spin of stellar mass BH is complementary to that of McClintock, Narayan & Shafee (2007). They use the soft high state when any power-law emission is minimal and fit the quasi-blackbody continuum spectrum. Their method, in contrast to ours, requires accurate measurements of the mass and distance of the BH. In the following section, we detail our analysis procedure and results.

2 OBSERVATION AND DATA REDUCTION

GX 339−4 was observed in its VHS by *XMM–Newton* for 75.6 ks, starting on 2002 September 29 09:06:42 UT (revolution 514) and simultaneously by *RXTE* for 9.6 ks starting at 09:12:11:28 UT (M1). LHS observations were made by *XMM–Newton* during revolutions 782 and 783, for a total exposure of 280 ks starting on 2004 March 16 16:23:41 TT and *RXTE* on 2004 March 17 at 12:03:12 TT, observation 90118-01-06-00 (M2). For the 2002 observation the EPIC-pn camera (Struder et al. 2001) was operated in 'burst' mode with a 'thin' optical blocking filter. For the low/hard observation the EPIC-MOS1 and EPIC-MOS2 cameras (Turner et al. 2001) were operated in the standard 'full-frame' mode with the 'medium' EPIC optical blocking filter in place. Starting with the unscreened level 1 data files for all the aforementioned observations, we followed the reduction procedures mentioned in M1 and M2.

In essence, for the *XMM–Newton* observation of the VHS the Observational Data Files (ODFs) were processed using the latest *XMM–Newton* Science Analysis System v 7.1.0 (SAS), with events being extracted in a stripe in RAWX (31.5–40.5) *versus* RAWY (2.5–178.5) space. Bad pixels and events too close to chip edges were ignored by requiring 'FLAG = 0' and 'PATTERN $\leqslant$ 4'. The energy channels were grouped by a factor of 5 to create a spectrum. The standard canned burst mode response file epn˙bu23˙sdY9˙thin.rsp was used to fit the spectrum. The total good exposure time selected was 2.2 ks. Due to the high source flux, background spectra were not extracted. *RXTE* data for the VHS were reduced using the *RXTE* tools provided in the HEASOFT v 5.2 software package. Standard time filtering, including the South Atlantic Anomaly and elevation angle restriction ($\geqslant 10^\circ$ from the Earth's limb) resulted in a net Proportional Counter Array (PCA) and High-Energy X-Ray Timing Experiment (*HEXTE*) exposures of 9.3 and 3.3 ks, respectively. To account for residual uncertainties in the calibration of PCU-2, we added 0.75 per cent systematic error to all its energy channels. The response matrix was made by the task 'pcarsp'. The *HEXTE* source and background spectra were made using the standard recipes. Standard canned responses were used for spectral fitting.

The *XMM–Newton* data from the 2004 LHS was reduced using SAS v 7.1.0. As opposed to the EPIC-pn data, the EPIC-MOS cameras in the 'full-frame' mode are more susceptible to photon

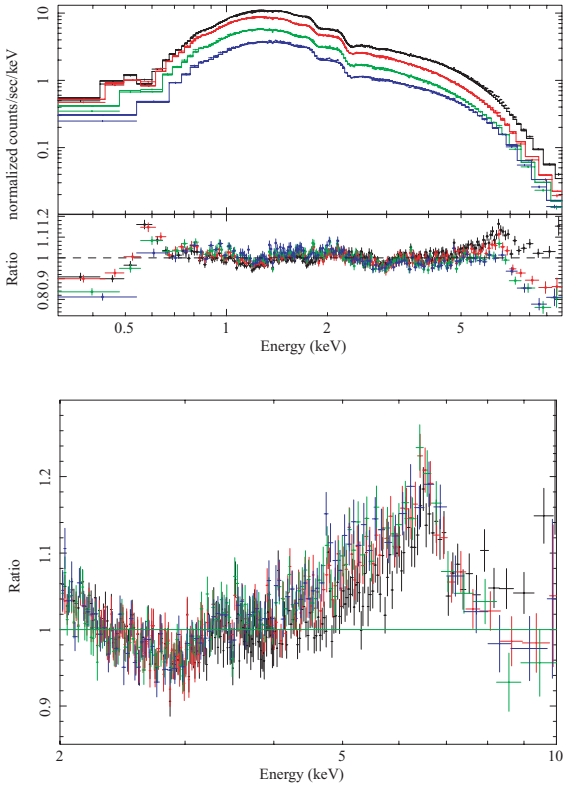

Figure 1. EPIC-MOS1, revolution 782 spectra for various source extraction regions and event selection criterion fitted with a simple power-law and MCD component (see text). Top (from top to bottom): Source extraction region in annulus with inner radius 18 arcsec single–quadruple pixel, 18 arcsec single pixel, 30 arcsec single pixel and 50 arcsec single–quadruple pixel. Bottom: Data/model ratio for the region around the iron line profile with a power law. The energy range 4.0–7.0 keV was ignored during the fit. It is clear that pile-up is only significantly present in the annular with inner radius 18 arcsec and both single–quadruple pixel (top black).

and pattern pile-up. Pile-up occurs when several photons hit two neighbouring (pattern pile-up) or the same (photon pile-up) pixel in the CCD before the end of a readout cycle. If this happen the events are counted as one single event having an energy equal to the sum of all their energies, thus hardening the spectra. In order to investigate the effect of pile-up suffered by the EPIC-MOS cameras, we used the SAS tool xmmselect to obtain spectra from annular regions of inner radius 18, 25, 30 and 50 arcsec and outer radius of 120 arcsec centred on the source. The events were filtered by requiring 'FLAG=0' and 'PATTERN $\leqslant$ 12' (single–quadruple pixel events) as well as 'PATTERN==0' (only single-pixel events). Background spectra were extracted from a 60 arcsec circle near the corner of the central chip of each MOS camera for both 'PATTERN $\leqslant$12' and 'PATTERN==0'. Response files for each spectrum were created using the tools rmfgen and arfgen. The FTOOL grppha was used to require at least 20 counts bin^{-1}. The spectra of four different extraction region and event criterion for the EPIC-MOS1 (revolution 782) observation are shown in Fig. 1, fitted with a simple power-law and MCD component modified by absorption in the interstellar medium (PHABS model in XSPEC). The various parameters were tied between the spectra and a normalization constant was allowed to float between them. It is clear from Fig. 1 that pile-up only significantly affects the spectrum created with the source extraction region with inner radius 18 arcsec and 'PATTERN$\leqslant$12'. All other spectra are consistent with the most conservative extraction region (inner

radius 50 arcsec, single-pixel events) at energies between 0.7 and 10.0 keV. The overall shape of the spectrum is, however, not significantly affected by pile-up in all extraction regions and patterns, as can be seen in the lower panel of Fig. 1.

In order to maximize signal-to-noise ratio and make use of the best calibrated response matrix for the LHS, we use the spectra extracted from the annulus with inner radius of 18 arcsec and single-pixel events throughout the analysis detailed in this work. A net exposure time of 56 and 59 ks was obtained in revolution 782 for the EPIC-MOS1 and EPIC-MOS2 camera, respectively, and 58 ks for each camera in revolution 783. For the *RXTE* data set, the reduction procedure involved the use of the tools provided in the *RXTE* HEASOFT v 6.0 software package. We used the 'Standard 2 mode' data from PCU-2 only. The event files and spectra were screened and the background and response files created. Systematic errors of 0.75 per cent were added to all PCU-2 energy channels. The *HEXTE*-A cluster was operated in the 'standard archive mode'. Background-subtracted spectrum and associated instrument response files were created using standard procedures. The *RXTE* observations resulted in net PCA and *HEXTE* exposures of 2.2 and 0.8 ks, respectively.

We restrict our spectral analyses of the *XMM–Newton* EPIC-pn data to the 0.7–9.0 keV band. For a preliminary constraint on the blackbody temperature of the LHS we use *XMM–Newton* EPIC-MOS data in the range 0.5–2.0 keV as we expect the temperature to be low; however, for the rest of the analyses *XMM–Newton* EPIC-MOS is used in the range 0.7–9.0 keV, similarly to the VHS, unless stated otherwise. The PCU-2 spectrum is restricted to the 2.8–25.0 keV band with an edge at 4.78 keV ($\tau = 0.1$) to account for the strong Xe *L* edge. *HEXTE* spectrum is analysed between 20.0 and 100.0 keV. A Gaussian line at 2.31 keV is introduced when fitting the EPIC-pn spectrum due to the presence of a feature at this energy that resembles an emission line. This feature is likely to be caused by Au M-shell edges and Si features in the detectors (M1). When fitting the *RXTE* spectra as well as the four spectra from the *XMM–Newton* low/hard observation (MOS1 and MOS2 for revolution 782 and 783), a joint fit is achieved by allowing a normalization constant to float between the various spectra. All parameters in fits involving different instruments were tied. XSPEC v 11.3.2 (Arnaud 1996) was used to analyse all spectra. The quoted errors on the derived model parameters correspond to a 90 per cent confidence level for one parameter of interest ($\Delta\chi^2 = 2.71$ criterion), unless otherwise stated.

3 ANALYSIS AND RESULTS

3.1 Fits to *RXTE* data: 2.8–100.0 keV continuum

We first analyse the *RXTE* PCU-2 and *HEXTE* spectra in order to constrain the power-law continuum of the two states. By considering the simplest power-law plus MCD model, modified by absorption in the interstellar medium (PHABS model in XSPEC) with an equivalent neutral hydrogen column density fixed at $N_{\rm H} = 5.3 \times 10^{21}$ cm^{-2} (Kong et al. 2000), resulted in a poor fit for both states, with $\chi^2/\nu = 279.5/74$ and 275.0/76 for the VHS and LHS, respectively. In the case of the LHS the addition of a MCD component did not affect the fit. Significant residual features are present in the region around the Fe Kα fluorescence line. In order to phenomenologically model a disc reflection line we initially added a Gaussian emission line and smeared edge components (SMEDGE in XSPEC) to the model. This significantly improved the fit with $\chi^2/\nu = 68.7/68$ and 88.9/70 for the VHS and LHS, respectively. The parameters measured in the VHS for this model are $\Gamma_{\rm PL} = 2.56^{+0.12}_{-0.08}$, $R_{\rm PL} = 2.7^{+1.5}_{-0.5}$, $kT = 0.87^{+0.02}_{-0.06}$ keV, $R_{\rm MCD} = 2200^{+1000}_{-300}$, $E_{\rm gauss} = 6.0^{+0.4}_{-1.0}$ keV, FWHM $= 2.6^{+0.9}_{-1.0}$ keV, $R_{\rm gauss} = 0.02^{+0.07}_{-0.01}$, EW $= 220 \pm 100$ ev, $E_{\rm SMEDGE} = 8.8^{+0.5}_{-1.7}$ keV, $\tau_{\rm SMEDGE} = 0.2^{+0.8}_{-0.2}$, $W_{\rm SMEDGE} = 2.0^{+3.0}_{-1.0}$ keV (where R is the normalization for each function). The equivalent parameters for the LHS are $\Gamma_{\rm PL} = 1.48 \pm 0.01$, $R_{\rm PL} = 0.204^{+0.005}_{-0.007}$, $E_{\rm gauss} = 5.9^{+1.2}_{-0.6}$ keV, FWHM $= 0.9^{+1.4}_{-0.5}$ keV, $R_{\rm gauss} = 1.7^{+2.8}_{-1.0} \times 10^{-3}$, EW $= 110 \pm 40$ ev, $E_{\rm SMEDGE} = 7.1^{+0.6}$ keV, $\tau_{\rm SMEDGE} = 0.3^{+0.2}_{-0.1}$, $W_{\rm SMEDGE} = 2.3 \pm 2.0$ keV. The values obtained for both states are in agreement with those in M1 and M2.

3.2 Fits to *XMM–Newton* EPIC-pn and MOS data

3.2.1 Verifying the presence of a quasi-blackbody component

Whilst fitting *XMM–Newton* data for both VHS and LHS, the power-law index was constrained to lie within $\Delta\Gamma \leqslant 0.1$ from the values obtained in the *RXTE* fits. We began by considering a simple power-law continuum plus blackbody component in the form of a MCD. The hydrogen column density was fixed at $N_{\rm H} = 5.3 \times 10^{21}$ cm^{-2} for both states. A fit to the VHS EPIC-pn data in the range 0.7–3.0 keV ($\chi^2/\nu = 1448.9/462$) shows the presence of a blackbody component with temperature of ≈0.76 keV (Fig. 2, top). We used EPIC-MOS data in the range 0.5–2.0 keV to verify the presence of a MCD component in the LHS. Fig. 2 (bottom) shows the data/model ratio (extended to an energy range of 5.0 keV) without a blackbody component for the LHS. The best-fitting model requires a disc blackbody with a temperature of ≈0.22, with $\chi^2/\nu = 1137.8/389$. The best fit without a quasi-blackbody gives $\chi^2/\nu = 129\,617.2/389$,

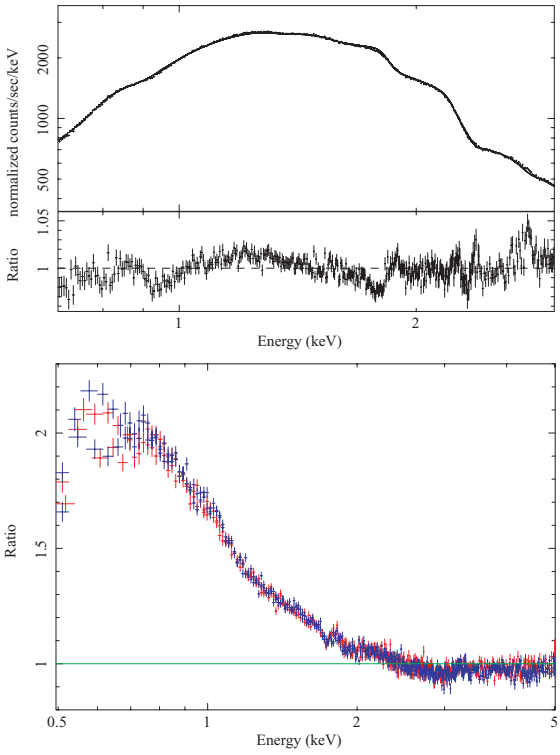

Figure 2. Top: Best-fitting spectra for the VHS showing the presence of a quasi-blackbody with a temperature of ≈0.76 keV (see text). Bottom: Data/model ratio without a quasi-blackbody component for the LHS. Revolution 782 and 783 are shown in red and blue, respectively (the data are combined for plotting purposes only). It is clear from these plots that a semiblackbody component is present in both states.

which clearly indicates the need for this component. Recently, similar results have been obtained for the low/hard state of GX 339−4, where an optically thick disc with a temperature of ≈0.2 keV has been reported (Tomsick et al. 2008).

3.2.2 *Simple model: 0.7–9.0 keV*

We fit both the VHS and LHS simultaneously with a power-law plus MCD component. Only the value of $N_{\rm H}$ was tied between the states. The best-fitting value found for $N_{\rm H}$ of $5.170 \pm 0.001 \times 10^{21}$ cm^{-2} is in accordance with that of Kong et al. (2000). We restricted the value of $N_{\rm H}$ to 5.1–5.3 $\times 10^{21}$ for the remainder of thus work. Fig. 3 shows the spectra with the data/model ratio. The formally unacceptable fit ($\chi^2/\nu = 10\,279.4/3860$) can be seen to be due mainly to the broad iron line and soft energy residuals, and for the VHS, a large Fe Kα absorption edge.

To provide a physically realistic description of the Fe line region we initially added a relativistic Fe line (LAOR, Laor 1991) to the MCD and power-law continuum and, for the VHS, a smeared edge to phenomenologically model the iron Kα absorption edge. The LAOR model describes a broad line from an accretion disc surrounding a rotating Kerr BH, with an emissivity profile described by a power law of the form $\epsilon_{(r)} = r^{-q}$. The outer disc radius was fixed at the maximum allowed value of $400r_{\rm g}$. The inner radius of the disc, $r_{\rm in}$, emissivity index, q, disc inclination, i, and the normalization were free to vary. It should be noted that constraining the spin based on the LAOR model, although robust, is only an approximation since the identification of $r_{\rm in}$, as determined from LAOR assumes a hard wired spin parameter of $a = 0.998$. The way that the inferred BH spin depends on the position of the inner radius was explored by Dovciak, Karas & Yaqoob (2004), and was shown to be consistent with the 'true' spin as one considers more rapidly rotating BHs (see their fig. 2). We fit both the VHS and LHS individually, restricting the value of $N_{\rm H}$ to $5.2 \pm 0.1 \times 10^{21}$ cm^{-2}. The fit parameters are given in Table 1. Adding both a LAOR and SMEDGE components significantly improved the fit for the VHS, with $\chi^2/\nu = 2478.1/1652$ and the LHS with $\chi^2/\nu = 3069.7/2376$ (Fig. 4). For the LHS, residuals below 2.0 keV indicates that the simple power-law plus MCD components, predominant in this range, is not a accurate description of the continuum, and a more complex reflection component should be present. If data below 2.0 keV are removed for this state, and the disc temperature, normalization and column density is frozen, Model 1 converges to $\chi^2/\nu = 2249.3/2031$. The energy range below 2.0 keV does not affect the direct measurement of the Fe Kα line profile since the LAOR function used to model the line only extends down to an energy of ≈3.5 keV (see Fig. 4). We note that the parameters values found here differ slightly from those of similar models in M1 and M2 likely due to the restriction

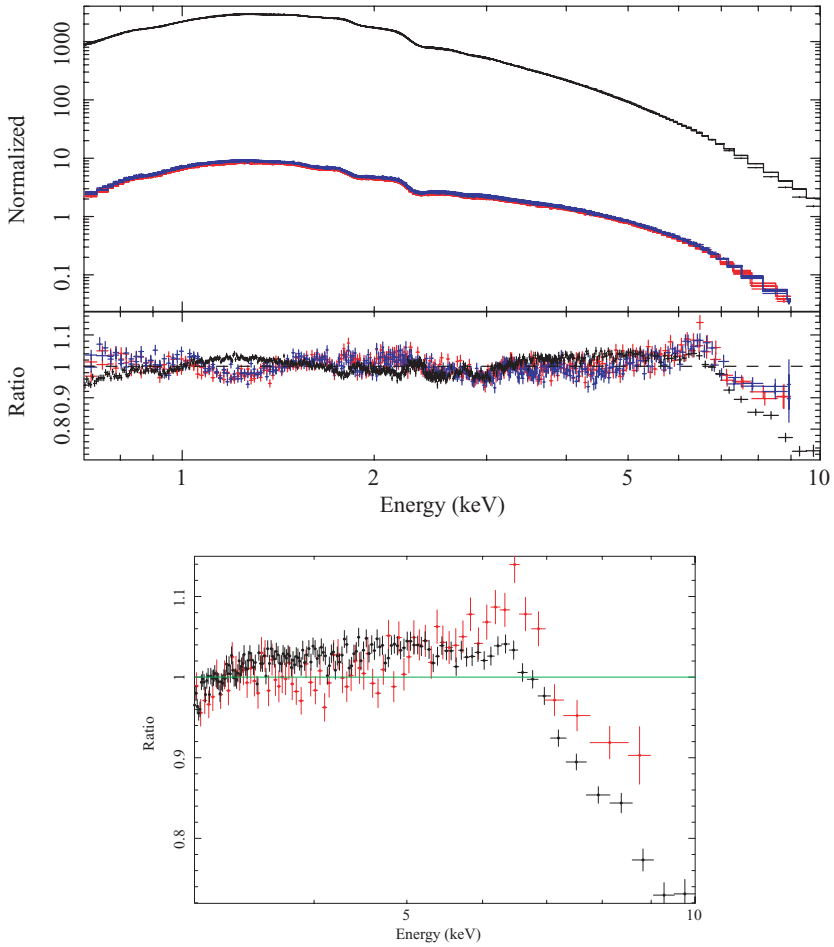

Figure 3. Top: Data/model ratio for a simple model consisting of a power-law and MCD components only. The *XMM–Newton* EPIC-pn data for the VHS are shown in black. Spectra for the combined EPIC-MOS (LHS) revolution 782 and 783 are shown in red and blue, respectively (the data are combined for plotting purposes only). Bottom: Blow-up of the EPIC-pn (black) and EPIC-MOS1 (revolution 782, red) spectrum showing the broad iron line and Fe Kα edge region. The data have been rebinned for visual clarity. The EPIC-pn spectrum has been extended to 10 keV for illustration purposes only.

Table 1. Results of fits to *XMM–Newton* EPIC-pn (VHS) and EPIC-MOS (LHS) data. The spectra were analysed in the 0.7–9.0 keV band.

Model 1 (PHABS × SMEDGE × [PL + DISKBB + LAOR])		
Parameter	Very high state	Low/hard state
$N_{\rm H}$ (10^{21} cm^{-2})	$5.300_{-0.004}$	$5.100^{+0.006}$
Γ	$2.567^{+0.004}_{-0.01}$	$1.700_{-0.002}$
$R_{\rm PL}$	$2.87^{+0.02}_{-0.01}$	0.231 ± 0.005
kT (keV)	0.721 ± 0.001	0.235 ± 0.02
$R_{\rm MCD}$	2890^{+10}_{-30}	8100 ± 300
$E_{\rm LAOR}(keV)$	$6.97_{-0.01}$	$6.97^{+0.01}_{-0.06}$
$q_{\rm LAOR}$	$6.82^{+0.03}_{-0.04}$	$3.23^{+0.05}_{-0.04}$
$r_{\rm in}$ ($r_{\rm g}$)	$1.91^{+0.02}_{-0.01}$	2.8 ± 0.1
$i(^\circ)$	$18.2^{+0.3}_{-0.5}$	$10.0^{+2.0}$
$R_{\rm LAOR}(\times 10^{-3})$	130 ± 2	3.75 ± 0.15
$E_{\rm SMEDGE}$(keV)	$7.10^{+0.01}$	–
$\tau_{\rm SMEDGE}$	$2.3^{+0.1}_{-0.6}$	–
$W_{\rm SMEDGE}$	4.1 ± 0.2	–
χ^2/ν	2478.1/1652	3069.7/2376

imposed on the neutral hydrogen column density, $N_{\rm H}$ and on improved calibration.

3.2.3 *More complex models: very high state*

In all our previous fits, the presence of a broad iron emission line has been determined and successfully modelled by the LAOR kernel. The presence of a possible edge at ≈7.1 keV found for the VHS is consistent with that predicted from absorption due to Fe *K*-shell transition in partially ionized, 'warm', material (Ross & Fabian 1993; Ross, Fabian & Brandt 1996). To date, BHB spectra have been modelled by a combination of a line model such as LAOR or KERRDISK (Brenneman & Reynolds 2006), a separate reflection function such as PEXRIV and a multicolour disc, since no self-consistent reflection model had been available. Here, we use the reflection model developed by Ross & Fabian (2007, REFHIDEN) to model those components jointly for the VHS. The parameters of the model are the number density of hydrogen in the illuminated surface layer, $H_{\rm den}$, the value of kT for the blackbody entering the surface layer from below, the power-law photon index, and the ratio of the total flux illuminating the disc to the total blackbody flux emitted by the disc. The disc reflection spectra is convolved with relativistic blurring kernel KDBLUR, which is derived from the code by Laor (1991). The power-law index of REFHIDEN is tied to that of the hard component. We constrain the value of $N_{\rm H}$, inclination, and power-law index to 5.1–5.3 × 10^{21} cm^{-2}, 10°–20° and 2.5–2.7 as found from Model 1 above. Using this model we obtained a much improved fit for the VHS, with $\chi^2/\nu = 2348.8/1655$ (Model 2). Allowing for a broken power law for the emissivity further improves the fit, with $\chi^2/\nu = 2237.8/1653$ (Model 3, see Fig. 5, top) and an *F*-Statistic value over the previous fit of 41, implying a probability of $<10^{-18}$ of a random occurrence. The parameters found for these models are shown in Table 2. A direct inspection of Fig. 5 (Top) shows the presence of a possible photoionization edge for O VIII at ≈0.86 keV and a narrow line at ≈6.4 keV. Adding an edge at 0.86 keV with an optical depth $\tau = 3.5^{+0.7}_{-0.9} \times 10^{-2}$, as well as a narrow Gaussian at 6.4 keV results in $\chi^2/\nu = 2144.9/1651$ (Fig. 5, bottom). The presence of the narrow Gaussian component is required at the 98 per cent level (*F*-test probability of 0.02) and can be attributed as due to reflection from distant materials. By looking at the contribution to χ^2 (not shown in Fig. 5) it is clear that the majority of the contribution comes from the energy range 1.6–3.3 keV and is likely the result of Au M-shell edges and Si features in the detector. Due to the high signal-to-noise ratio achieved, these features are clearly revealed and thus affect the overall χ^2 fit statistics but not the values of the best-fitting parameters.

From the irradiating source luminosity, $L_{\rm x}$ (defined here between 0.2 and 10.0 keV), disc hydrogen density ($H_{\rm den}$) and radius, R (approximated to $2.0r_{\rm in}$), it is possible to estimate the ionization parameter ($\xi = L_{\rm x}/H_{\rm den}\,R^2$), of the VHS as $\log \xi \approx 4.2$, which is consistent with previous values found for GX 339−4 in its very high state (M1). Using a self-consistent reflection model we were able to constrain the value of the innermost radius to $r_{\rm in} = 2.03^{+0.025}_{-0.035} r_{\rm g}$. This strong constraint can be better appreciated in Fig. 6, where the 90 per cent confidence lever for $r_{\rm in}$ is shown as the dashed line in the χ^2 plot, obtained with the 'steppar' command in XSPEC. Assuming that $r_{\rm in} = r_{\rm ms}$ we get a spin parameter $a/M = 0.939^{+0.004}_{-0.003}$ for the VHS.

It should be noted that the measured values for the disc temperature found by the REFHIDEN model is at least 0.15 keV less than the value obtained via fits with the additive components (Model 1). This behaviour is as expected (see Merloni et al. 2000; Ross & Fabian 2007)) since in Model 1 the soft disc component is modelled with a multicolour disc quasi-blackbody (DISKBB) having a Comptonized surface colour–temperature ($T_{\rm col}$) intrinsically higher than the effective mid-plane temperature ($T_{\rm eff}$) used in

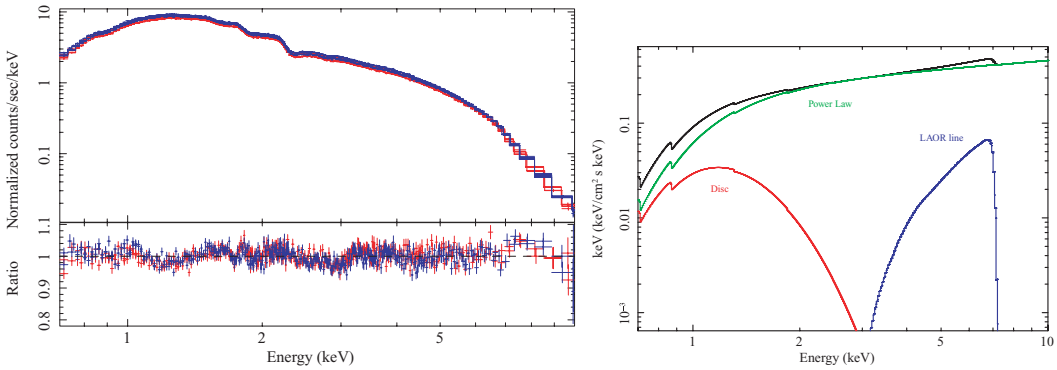

Figure 4. Left-hand panel: LHS data/model ratio for a model consisting of a simple power-law and MCD components, as well as a LAOR line (Model 1). Spectra for the combined EPIC-MOS revolution 782 and 783 are shown in red and blue, respectively. The data are combined and rebinned for plotting purposes only. Right-hand panel: Model components for MOS1 revolution 782.

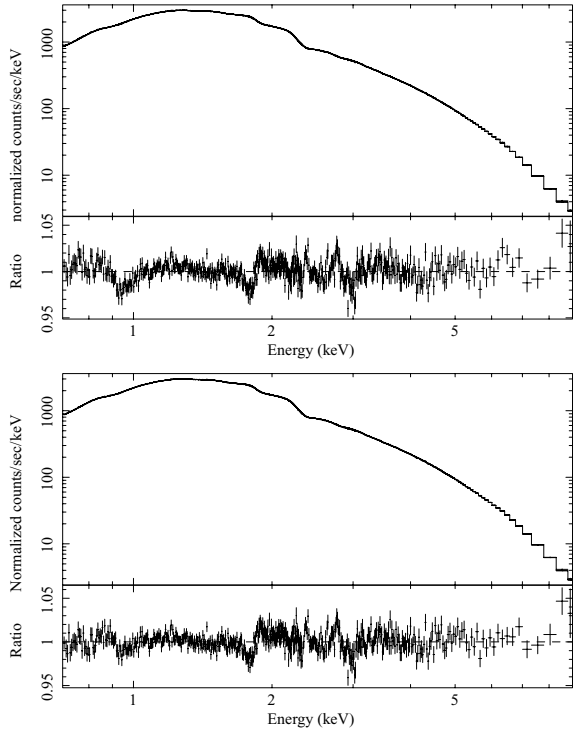

Figure 5. Data/model ratio for the VHS. Top: Model assumes a broken power-law emissivity profile and constitute of a power law and the disc reflection function REFHIDEN. The presence of a O VIII edge at 0.86 keV and a possible narrow emission line at ≈6.4 keV can be seen. Bottom: Same as above but with an additional narrow Gaussian line and a O VIII edge at 0.86 keV. The data have been rebinned for visual clarity.

Table 2. Result of more complex fits to *XMM–Newton* EPIC-pn data for GX 339−4 in the very high state.

Parameter	Model 2	Model 3
$N_{\rm H}$ (10^{21} cm^{-2})	5.16 ± 0.02	5.17 ± 0.03
Γ	$2.7_{-0.01}$	$2.7_{-0.02}$
$R_{\rm PL}$	$1.45^{+0.25}_{-0.15}$	$2.8^{+0.2}_{-0.3}$
kT (keV)	$0.519^{+0.006}_{-0.01}$	0.554 ± 0.004
$H_{\rm den}(\times 10^{21}$ H cm$^{-3})$	4.05 ± 0.2	$4.52^{+0.4}_{-0.2}$
Illum/BB	$4.4^{+0.4}_{-0.3}$	2.0 ± 0.1
$R_{\rm REFHIDEN}$	$4.4^{+0.2}_{-0.1}$	$2.7^{+0.1}_{-0.3}$
$q_{\rm in}$	$6.84^{+0.1}_{-0.2}$	$7.6^{+0.3}_{-0.6}$
$q_{\rm out}$	–	$3.7^{+0.3}_{-0.8}$
$r_{\rm break}(r_g)$	–	$4.9^{+0.6}_{-0.7}$
$r_{\rm in}$ ($r_{\rm g}$)	$1.804^{+0.08}_{-0.004}$	$2.03^{+0.025}_{-0.035}$
i (°)	$19.5^{+0.5}_{-3}$	$19.98^{+0.02}_{-0.7}$
χ^2/ν	2348.8/1655	2237.8/1653

Notes: Model 2 is described in XSPEC as PHABS × (KDBLUR × [PL + REFHIDEN]). Model 3 assumes the accretion disc has a broken power-law emissivity profile described by the function KDBLUR2 in XSPEC. The value of $N_{\rm H}$, inclination, and power-law index was constrained to 5.1–5.3 × 10^{21} cm^{-2}, 10°–20° and 2.5–2.7, respectively, in both models.

REFHIDEN. The spectral hardening factor $f_{\rm col} = T_{\rm col}/T_{\rm eff}$ (Shimura & Takahara 1995) of ≈1.3 found for the VHS is very similar to the conventional value of 1.7 ± 0.2 (Shimura & Takahara 1995). It is expected that a similar reduction in the value of kT should occur for the LHS where the effective disc temperature would be less than the value found in Section 3.3.1 of ≈0.22 keV.

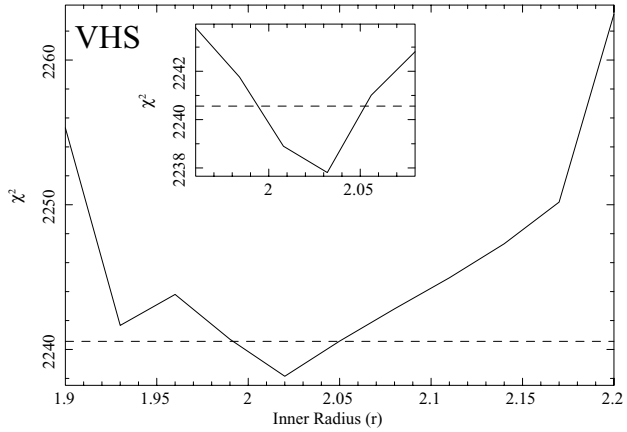

Figure 6. χ^2 versus $r_{\rm in}$ plot for GX 339−4 in its very high state. A value of $r_{\rm in} = 2.03^{+0.025}_{-0.035} r_{\rm g}$ is found at the 90 per cent confidence level for one parameter, $\Delta\chi^2 = 2.71$ criterion shown by the dashed line. The inset shows a close up of the region around the χ^2 minima.

3.2.4 More complex models: low/hard state

The effective temperature of around 0.15 keV and hydrogen number density $H_{\rm den} > 2 \times 10^{21}$ H cm^{-3} expected for the LHS falls outside the parameter range of the REFHIDEN model. However, the model is being developed and an analysis of the LHS with REFHIDEN is left for future work. The disc blackbody in the LHS has a negligible effect on the iron Kα features above 2.0 keV (see Fig. 4). For comparison with our results for the VHS, we use REFLIONX to analyse *XMM–Newton* EPIC-MOS data for the LHS in the range 2.0–10.0 keV with a model similar to REFHIDEN but lacking the intrinsic blackbody disc component. The model REFLIONX is a revised version of REFLION (Ross & Fabian 2005) used to describe reflection from accretion disc in AGN systems where the blackbody emission is at too low an energy to affect the Fe Kα emission. It should be stressed that the reflection features above 2 keV are unlikely to be significantly affected by the change from REFHIDEN to REFLIONX. The parameters of the model are the iron abundance (set to solar), photon index of the illuminating power law, ionization parameter, ξ, and the normalization. The disc reflection spectra are convolved with the relativistic blurring kernel, KDBLUR. The power-law index in REFLIONX is tied to that of the hard component. We constrain the value of the inclination, and power-law index to 10°–20° and 1.4–1.6, respectively. The hydrogen column density, $N_{\rm H}$ is fixed at 5.17 × 10^{21} cm^{-2}, the best-fitting value found for the VHS, as we do not expect it to vary. The best fit obtained with the blurred REFLIONX model is shown in Fig. 7 and detailed in Table 3. This model gives $\chi^2/\nu = 2242.5/2031$ with an emissivity index of 3.065 ± 0.05 indicating a standard 'lamppost' emissivity profile. The value found for the inclination of $20^{\circ}_{-1.7}$ is in agreement with that for the VHS. The low disc ionization parameter, log(ξ)≈3, is consistent with that expected for low disc temperatures. At 90 per cent confidence, this model gives constraint on the innermost stable radius of $r_{\rm in} = 2.08^{+0.17}_{-0.10}$ $r_{\rm g}$ (see Fig. 8). If we include the energy band 0.7–2.0 keV to the above fit, a large low-energy residual is present due to the disc emission. By modelling this with a DISKBB component, a best fit of $\chi^2/\nu = 3070.9/2388$ is achieved in the full 0.7–10.0 keV range with a disc temperature of 0.201 ± 0.003 keV as in Section 3.2.1.

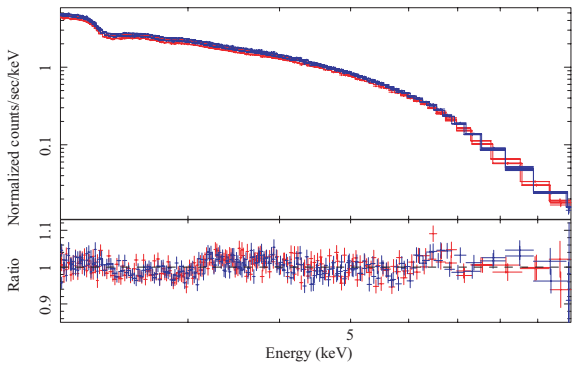

Figure 7. LHS data/model ratio for a relativistic blurred disc reflection model (REFLIONX) and power law as described in the text. The spectra for the combined EPIC-MOS revolution 782 and 783 are shown in red and blue, respectively. The data have been combined and rebinned for plotting purposes only.

Table 3. Results of fits to *XMM–Newton* EPIC-MOS data for the low/hard state of GX 339−4. The spectra was analysed in the 2.0–10.0 keV band. $N_{\rm H}$ was fixed at the quoted value.

Parameter	Low/hard state
$N_{\rm H}$ (10^{21} cm^{-2})	5.17
Γ	$1.48^{+0.09}_{-0.08}$
$R_{\rm PL}$	0.11 ± 0.01
q	3.065 ± 0.05
$r_{\rm in}$ ($r_{\rm g}$)	$2.08^{+0.17}_{-0.10}$
i (°)	$20_{-1.7}$
ξ(erg cm s^{-1})	1350 ± 100
$R_{\rm REFLIONX}$($\times$ 10^{-6})	$4.0^{+0.4}_{-1.0}$
χ^2/ν	2242.5/2031

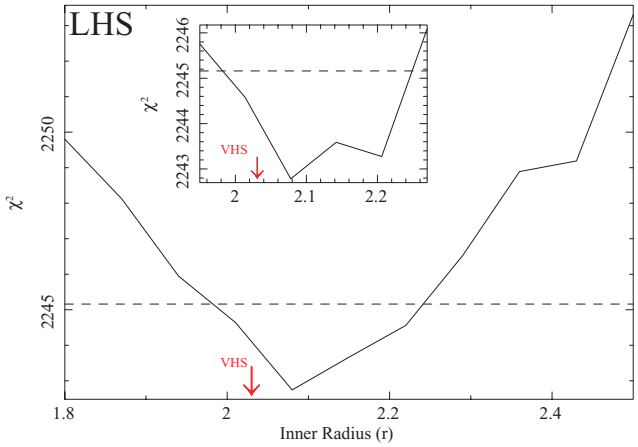

Figure 8. χ^2 versus $r_{\rm in}$ plot for GX 339−4 in its low/hard state. An inner radius, $r_{\rm in} = 2.08^{+0.17}_{-0.10} r_{\rm g}$ is found at the 90 per cent confidence level for one parameter, $\Delta\chi^2 = 2.71$ criterion shown by the dashed line. The inset shows how χ^2 behaves closer to the minima. The inner radius found for the VHS is shown in red for comparison.

3.3 Joint *XMM–Newton – RXTE* spectrum analysis

3.3.1 Very high state: 0.7–100.0 keV

In order to check the robustness of our results, we extended the fit from the EPIC-pn spectrum to include the energy range 0.7–100 keV, using *RXTE* data. PCU-2 data were fitted between 8.0 and 25.0 keV. This resulted in a poor fit, with $\chi^2/\nu = 4017.0/1727$. It should be stressed that the quality of the EPIC-pn data far outweights that of *RXTE* and thus a statistically worst fit is inevitable in the full range. However, most of the residuals are accounted for by allowing the power-law index to vary. The best-fitting value of $\Gamma = 2.583 \pm 0.007$ is in accordance to that found in Section 3.1 for the *RXTE* continuum. The parameters for fits to the combined EPIC-pn and *RXTE* spectrum are listed in Table 4 and shown in Fig. 9 (left-hand panel). It is clear that the model is a very good description of the spectrum (see Fig. 9), with $\chi^2/\nu = 2549.3.0/1718$ in the full 0.7–100.0 keV range. Most importantly, the value for the inner radius, $r_{\rm in}$ found here of $2.02^{+0.02}_{-0.06}$ $r_{\rm g}$ is similar to that found in Section 3.2.3.

Table 4. Joint *XMM–Newton* and *RXTE* spectral fits with relativistic blurred disc reflection models.

Parameter	Very high state	Low/hard state
$N_{\rm H}$(10^{21} cm^{-2})	$5.100^{+0.004}$	5.17
Γ	2.583 ± 0.007	$1.43^{+0.005}_{-0.02}$
$R_{\rm PL}$	$2.61^{+0.13}_{-0.09}$	$0.094^{+0.005}_{-0.004}$
kT(keV)	0.585 ± 0.001	–
$H_{\rm den}$($\times 10^{21}$ H cm^{-3})	6.6 ± 0.2	–
Illum/BB	1.00 ± 0.02	–
ξ(erg cm s^{-1})	$>10\,000$	1330^{+70}_{-60}
$R_{\rm REFHIDEN}$	$1.92^{+0.02}_{-0.06}$	–
$R_{\rm REFLIONX}$(10^{-6})	–	4.4 ± 0.2
$q_{\rm in}$	$7.05^{+0.05}_{-0.20}$	3.16 ± 0.05
$q_{\rm out}$	$3.0^{+0.1}$	–
$r_{\rm break}$(r_g)	$6.0^{+0.2}_{-0.1}$	–
$r_{\rm in}$ ($r_{\rm g}$)	$2.02^{+0.02}_{-0.06}$	$2.04^{+0.07}_{-0.02}$
i (°)	$20.0_{-0.3}$	$20.0_{-1.3}$
χ^2/ν	2549.3/1718	2316.6/2095

Notes: VHS was modelled with REFHIDEN and a broken power-law emissivity profile, as described in the text. For the LHS, the disc reflection model REFLIONX was used, and the spectra was fitted in the range 2–100 keV.

3.3.2 Low/hard state: 2–100 keV

A similar extension on the energy range of the LHS was made, with *RXTE* data being used in conjunction with EPIC-MOS. A best fit of $\chi^2/\nu = 2316.6/2095$ over the full 2.0–100.0 keV energy band is found. The various parameters are shown in Table 4 and the resulting spectra in Fig. 9 (right-hand panel). The value for the inner radius, $r_{\rm in}$ found here of $2.04^{+0.07}_{-0.02} r_{\rm g}$ is similar to that found in Section 3.2.4.

4 DISCUSSION

The spectral modelling of the VHS suggests that the surface layer of the accretion disc is highly ionized, with $\xi \sim 10^4$ erg cm s^{-1}. In this state, the iron in the outer layer of the disc is fully ionized and regions $\gtrsim$2 Thomson mean free paths below the surface produces a strong iron K absorption edge. Narrow Kα line emission from this region is then Compton-broadened as it scatters out of the disc. The strong presence of the iron K edge in the VHS can be seen in Fig. 3 and quantitatively appreciated by the high optical depth ($\tau = 2.3^{+0.1}_{-0.6}$) of the (phenomenological) component SMEDGE in

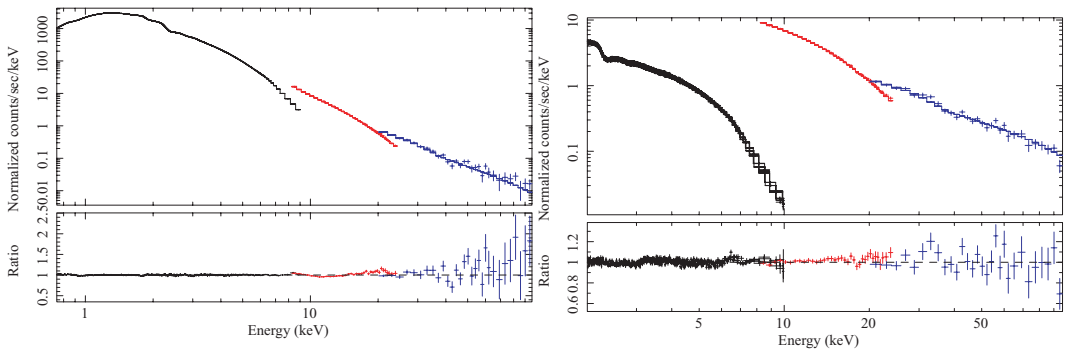

Figure 9. *XMM–Newton* and *RXTE* spectra of GX 339−4, fit jointly with a disc reflection model convolved with the relativistic blurring kernel, KDBLUR. Left-hand panel: VHS spectrum in the 0.7–100.0 keV range. Right-hand panel: LHS spectrum in the 2.0–100.0 keV range. The best fit indicates a value for $r_{\rm in}$ of $2.02^{+0.02}_{-0.06} r_{\rm g}$ and $2.04^{+0.07}_{-0.02} r_{\rm g}$ for the VHS and LHS, respectively. EPIC-MOS/pn data are shown in black. *RXTE* PCU-2 and *HEXTE* data are shown in red and blue, respectively. The data have been rebinned for visual clarity.

Model 1. The best-fitting REFHIDEN model clearly shows the large K-shell absorption feature and weak Kα emission line characteristic of the VHS in GX 339−4 (Fig. 10, left-hand panels). Note that similar features have also been observed in the VHS of Cygnus X-1 (Done et al. 1992). The ionization parameter found for the LHS, $\xi = 1350 \pm 100\,{\rm erg\,cm\,s^{-1}}$, is consistent with the disc being moderately ionized and having a low apparent temperature. In this state, the illuminated accretion disc results in a strong Fe Kα line emission from the top layers. Compton-broadening, although present, cannot explain the highly broadened and skewed line shape (see Fig. 3), where the low-energy red wing extend down to $\approx$4 keV. Fig. 10 (right-hand panels) shows the best-fitting REFLIONX model, prior to (top) and after blurring (bottom), for the LHS. As opposed to the VHS, in the low/hard state the Fe Kα line is clearly seen. The value for the ionization parameter for the low/hard state of $\xi \sim 10^4\,{\rm erg\,cm\,s^{-1}}$ reported by Tomsick et al. (2008) is an order of magnitude higher than the present result. At these values, the iron is fully ionized and should not produce an iron Kα reflection line (Matt, Fabian & Ross 1993; Young, Ross & Fabian 1998). The apparent inconsistency in their results can be attributed to the use of PEXRIV (Magdziarz & Zdziarski 1995) as the reflection model. This model does not account for diffusion of photons in the disc and thus rectify broadening caused by Comptonization by increasing the ionization parameter.

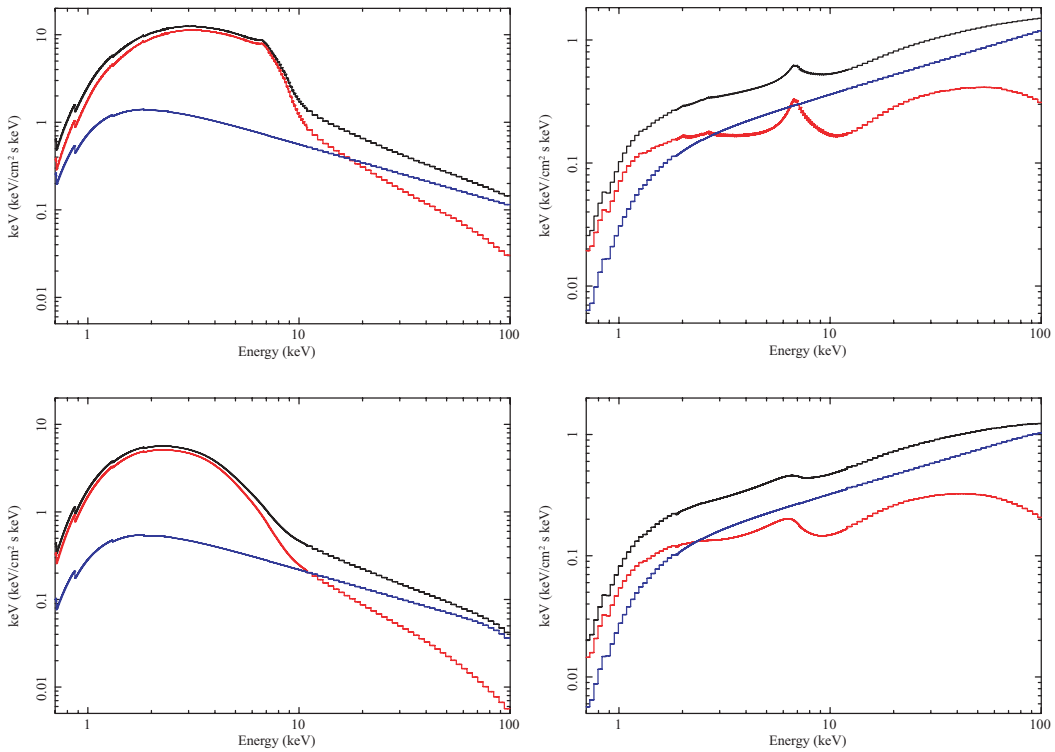

Figure 10. Top: Best-fitting model components prior to blurring for the VHS (left-hand side) and LHS (right-hand side). The combined model, reflection, and power-law components are shown in black, red and blue, respectively. Iron is fully ionized in the VHS, thus resulting in a very small Fe Kα line emission and a large iron K absorption edge. In the LHS, moderate ionization means that the contribution to the spectra from Fe Kα line emission is greater (see text). For the LHS, we only show EPIC-MOS1 revolution 782 for visual clarity. Bottom: Same as above, with relativistic blurring.

The obvious differences in the resulting spectra of the two states can be ascribed to the different ionization states of the disc. Previous attempts to model the spectra of Galactic BHB used the relativistic blurring of the Kα line to obtain the innermost radius, $r_{\rm in}$ and thus the spin parameter. In the present work, the full reflection spectra for the two extreme states was convolved, and the blurring parameters were obtained not just from the Kα line but from all of the reflection features. This is particularly important in the case of the VHS, where the Fe Kα emission line is not the dominant feature of the reflection component and Compton scattering needs to be fully accounted in the reflection model. In this state, a steep inner disc emissivity index of $q_{\rm in} = 7.6^{+0.3}_{-0.6}$, within a radius $r_{\rm break} = 4.9^{+0.6}_{-0.7}$ $r_{\rm g}$ is required, indicating that the corona is centrally concentrated. The model constrains the inner radius of the accretion disc to $r_{\rm in} = 2.03^{+0.025}_{-0.035} r_{\rm g}$ at the 90 per cent confidence level. It should be noted that the value for $r_{\rm in}$ quoted above for the *XMM–Newton* observation is consistent with that found for the full *XMM–Newton* plus *RXTE* fits, indicating that the model is an accurate description of both the reflection features as well as the underlying continuum. Assuming that emission within the innermost stable orbit is negligible (see Reynolds & Fabian 2008), the value of $r_{\rm in}$ found here translates to a BH spin of $0.939^{+0.004}_{-0.003}$ for the VHS. In the LHS, spectral fitting using the model REFLIONX resulted in an inner radius of $r_{\rm in} = 2.08^{+0.17}_{-0.10} r_{\rm g}$. This translates to a spin parameter of $0.93^{+0.015}_{-0.02}$ for the LHS.

The value for the spin parameter found for both states of GX 339−4 are within one per cent of one another and falls within 1σ error. It has been argued that bleeding of the iron line emission to regions inside the innermost stable radius may cause systematic errors in the derived value of the spin parameter (Reynolds & Begelman 1997; Krolik 1999). Using a high-resolution 3D MHD simulation of a geometrically thin accretion disc, Reynolds & Fabian (2008) have shown that the ionization edge is within $\sim 0.5 r_{\rm g}$ of the innermost stable circular orbit for a non-spinning BH. However, it was shown by the same authors that this bleeding decreases as the position of the innermost radius approaches the event horizon, and hence the spin inferred from the position of $r_{\rm in}$ becomes much closer to the true spin as one considers more rapidly rotating BHs. Similar results were reported by Dovciak et al. (2004, see their fig. 2). In order to verify our results against any systematic variation, we modelled the VHS with a KERRDISK line profile (Brenneman & Reynolds 2006). The spin, which is a free parameter of the model, was found to be $0.952^{+0.005}_{-0.001}$, lying within $\approx$1 per cent of the value inferred from the innermost radius.

The reflection model, REFHIDEN, assumes a single-temperature accretion disc. Although this is not a realistic claim, we believe it unlikely to have any significant effect on the inferred innermost radius of emission. In order to verify this hypothesis, we approximated a 'real' disc with inner radius increasing logarithmically from $2r_{\rm g}$ to $6.78r_{\rm g}$. Each point on the disc was assumed to radiate like a blackbody with an effective temperature that scales with radius as $r^{-3/4}$ starting at 0.9 keV. Within this region, the illuminating flux scaled as r^{-6}. Using the EPIC-pn response file, we modelled 1 ks of simulated data with a single temperature REFHIDEN. As expected, the model constrained the various parameter, with an effective temperature of $\approx$0.52 keV and an inner radius of $2.041^{+0.004}_{-0.020} r_{\rm g}$. As a further check on any inconsistency that may arise from using a single temperature disc reflection model to constrain the spin of the BH, we investigated the VHS with a different thermal model, (KERRBB, Li et al. 2005), which includes relativistic smearing in a disc with radial temperature gradient. The BH spin, a free parameter in the *KERRBB* model, was found to be 0.93 ± 0.02, consistent with that inferred from the single temperature REFHIDEN model.

5 CONCLUSIONS

We have analysed *XMM–Newton* spectra of GX 339−4 in both its very high and low/hard states. Looking at the difference in the spin parameter between the two states, as well as that derived from the various independent models for the VHS, we can estimate the systematic error in the iron line method to be about 1 per cent. By using a reflection model which intrinsically accounts for Comptonization and blackbody emission, we infer that the spin parameter of GX 339−4 is 0.935 ± 0.01 (statistical) ± 0.01 (systematic).

ACKNOWLEDGMENTS

RCR and GM acknowledge STFC for financial support. ACF and RR thanks the Royal Society and the College of the Holy Cross, respectively. CR thanks the US National Science Foundation for support under grant AST 06-07428.

REFERENCES

Arnaud K. A., 1996, in Jacoby G. H., Barnes J., eds, ASP Conf. Ser. Vol. 101, Astronomical Data Analysis Software and Systems V. Astron. Soc. Pac., San Francisco, p. 17
Bardeen J. M., Press W. H., Teukolsky S. A., 1972, ApJ, 178, 347
Brenneman L. W., Reynolds C. S., 2006, ApJ, 652, 1028
Done C., Mulchaey J. S., Mushotzky R. F., Arnaud K. A., 1992, ApJ, 395, 275
Dovciak M., Karas V., Yaqoob T., 2004, ApJ, 153, 205
Fabian A. C., Rees M. J., Stella L., White N. E., 1989, MNRAS, 238, 729
Fabian A. C., Iwasawa K., Reynolds C. S., Young A. J., 2000, PASP, 112, 1145
Hynes R. I., Steeghs D., Casares J., Charles P. A., O'Brian K., 2003, ApJ, 583, L95
Kong A. K. H., Kuulkers E., Charles P. A., Homer L., 2000, MNRAS, 312, L49
Krolik J. H., 1999, ApJ, 515, L73
Laor A., 1991, ApJ, 376, 90
Li L.-X., Zimmerman E. R., Narayan R., McClintock J. E., 2005, ApJS, 157, 335
Magdziarz P., Zdziarski A. A., 1995, MNRAS, 273, 837
Matt G., Fabian A. C., Ross R. R., 1993, MNRAS, 264, 839
McClintock J. E., Remillard R. A., 2006, in Lewin W. H. G., van der Klis M., eds, Cambridge Astrophys. Ser. Vol. 39, Compact Stellar X-ray Sources. Cambridge Univ. Press, Cambridge, p. 157
McClintock J. E., Narayan R., Shafee R., 2007, in Livio M., Koekemoer A., eds, Black Holes. Cambridge Univ. Press, Cambridge, in press (arXiv:0707.4492)
Merloni A., Fabian A. C., Ross R. R., 2000, MNRAS, 313, 193
Miller J. M., 2007, ARA&A, 45, 441
Miller J. M. et al., 2004, ApJ, 606, L131
Miller J. M., Homan J., Steeghs D., Rupen M., Hunstead R. W., Wijnands R., Charles P. A., Fabian A. C., 2006, ApJ, 653, 525
Miller J. M. et al., 2008, ApJL, in press (arXiv:0802.3882)
Mitsuda K. et al., 1984, PASJ, 36, 741
Munoz-Darias T., Casares J., Martinez-Pais I. G., 2008, MNRAS, 385, 2205
Reynolds C. S., Begelman M. C., 1997, ApJ, 448, 109
Reynolds C. S., Fabian A. C., 2008, ApJ, 675, 1048
Ross R. R., Fabian A. C., 1993, MNRAS, 261, 74
Ross R. R., Fabian A. C., 2005, MNRAS, 358, 211
Ross R. R., Fabian A. C., 2007, MNRAS, 381, 1697

Ross R. R., Fabian A. C., Brandt W. N., 1996, MNRAS, 278, 1082
Shimura T., Takahara F., 1995, ApJ, 445, 780
Struder L. et al., 2001, A&A, 365, L18
Tomsick A. J. et al., 2008, ApJ, in press (arXiv:0802.3357)
Thorne K. S., 1974, ApJ, 191, 507
Turner M. J. L. et al., 2001, A&A, 365, L27
Young A. J., Ross R. R., Fabian A. C., 1998, MNRAS, 300, L11
Zdziarski A. A., Gierlinski M., 2004, Prog. Theor. Phys. Suppl., 155, 99
Zdziarski A. A., Gierlinski M., Mikolanjewska J., Wardzinski G., Smith D. M., Harmon A., Kitamoto S., 2004, MNRAS, 351, 791

This paper has been typeset from a TEX/LATEX file prepared by the author.